

Spatially resolving the hot CO around the young Be star 51 Ophiuchi[★]

E. Tatulli^{1,2}, F. Malbet², F. Ménard², C. Gil³, L. Testi^{1,4}, A. Natta¹, S. Kraus⁵, P. Stee⁶, and S. Robbe-Dubois⁷

¹ INAF-Osservatorio Astrofisico di Arcetri, Istituto Nazionale di Astrofisica, Largo E. Fermi 5, I-50125 Firenze, Italy

² Laboratoire d'Astrophysique de Grenoble, UMR 5571 Université Joseph Fourier/CNRS, BP 53, F-38041 Grenoble Cedex 9, France

³ European Southern Observatory, Casilla 19001, Santiago 19, Chile

⁴ ESO, Karl-Schwarzschild Strasse 2, D-85748 Garching bei Muenchen, Germany

⁵ Max Planck Institut für Radioastronomie, Auf dem Hügel 69, 53121 Bonn, Germany

⁶ UMR 6525 CNRS H. FIZEAU UNS, OCA, Campus Valrose, F-06108 Nice cedex 2, France, CNRS - Avenue Copernic, Grasse, France.

⁷ Laboratoire Universitaire d'Astrophysique de Nice, UMR 6525 Université de Nice/CNRS, Parc Valrose, F-06108 Nice cedex 2, France

Received ; accepted

ABSTRACT

Aims. 51 Oph is one of the few young Be stars displaying a strong CO overtone emission at 2.3 microns in addition to the near infrared excess commonly observed in this type of stars. In this paper we first aim to locate the CO bandheads emitting region. Then, we compare its position with respect to the region emitting the near infrared continuum.

Methods. We have observed 51 Oph with AMBER in low spectral resolution ($R=35$), and in medium spectral resolution ($R=1500$) centered on the CO bandheads.

Results. The medium resolution AMBER observations clearly resolve the CO bandheads. Both the CO bandheads and continuum emissions are spatially resolved by the interferometer. Using simple analytical ring models to interpret the measured visibilities, we find that the CO bandheads emission region is compact, located at $0.15_{-0.04}^{+0.07}$ AU from the star, and that the adjacent continuum is coming from a region further away ($0.25_{-0.03}^{+0.06}$ AU). These results confirm the commonly invoked scenario in which the CO bandheads originate in a dust free hot gaseous disk. Furthermore, the continuum emitting region is closer to the star than the dust sublimation radius (by at least a factor two) and we suggest that hot gas inside the dust sublimation radius significantly contributes to the observed $2 \mu\text{m}$ continuum emission.

Key words. Techniques: interferometric – Stars: individual: 51 Oph – planetary systems: protoplanetary disks

1. Introduction

The environment of young stars is formed by a dusty and gaseous circumstellar disk in which the first stages of planet formation are thought to take place. Hence, building a comprehensive picture of the physical mechanisms governing this formation requires the understanding of the distribution and the evolution of both the dust and gas species. The content and dynamics of the gaseous component, which dominates the total mass of the disk, control the accretion-ejection processes and will define the final architecture of forming planetary systems. On the other hand, the dust, responsible for the continuum infrared excess, plays an essential role in determining the structure of the protoplanetary disk itself, since its opacity dominates in the continuum. Dust grains are also the first building blocks that will grow into kilometric planetesimals and then into eventual planets.

To study the planet formation taking place in the very inner region of the disk, one needs to combine milli-arcsecond high angular resolution techniques with high spectral resolution in order to directly probe the physical processes at stake both in the continuum and in the emission lines. In this respect,

near infrared spectro-interferometry that associates long baseline near infrared interferometry with spectroscopy appears perfectly suited. This technique indeed offers a unique way to spatially resolve both the continuum infrared excess and emission line components, that is to locate the regions of emission independently of any prior assumption regarding the physical mechanisms at play. In that sense, infrared spectro-interferometry has already provided important results about the origin of the hydrogen line Bry. Different authors have thus located the Bry emission region, showing that it can arise either from the accreting columns of gas falling onto the star (Eisner, 2007) or from outflowing winds in which ionized matter is ejected from the star (Malbet et al., 2007; Tatulli et al., 2007b; Kraus et al., 2008).

In this paper we are interested in exploring lines which are more direct probes of gas in the disk itself. We present the first interferometric observations of the $2.3\mu\text{m}$ CO overtone emission in the (B9) Be star 51 Oph. 51 Oph is one of the very few young stars where this emission is strong enough to be observed with infrared spectro-interferometry (Thi et al., 2005; Berthoud et al., 2007). This star exhibits also a strong Bry emission, which, assuming a magnetospheric origin (Muzerolle et al., 2004), indicates an accretion rate of $\dot{M} = 1 - 2 \cdot 10^{-7} M_{\odot}/\text{yr}$ (Garcia Lopez et al., 2006; Brittain et al., 2007). The dust component is rather compact (Lagage & Pantin (1994); Liu et al. (2007)) and shows a strong silicate feature in emission (Bouwman et al., 2001) but

Send offprint requests to: Eric.Tatulli@obs.ujf-grenoble.fr

[★] Based on ESO/VLTI programs 077.C-0706 and 60.A-9054

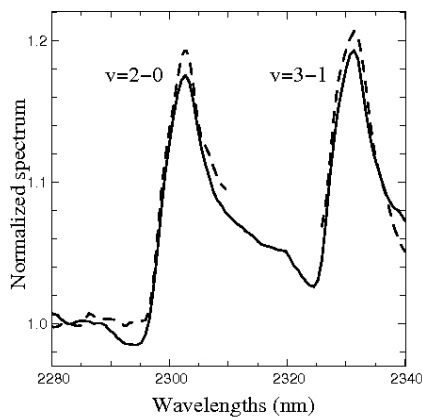


Fig. 1. AMBER calibrated spectrum of 51 Oph around the 2-0 and 3-1 bands of the CO overtone at 2.3 microns. For comparison purposes is plotted (dashed line) the same spectrum measured with the TNG spectrograph (L. Testi, private communication). Note that we did not plot the TNG spectrum between the two bandheads because of irrelevant instrumental artifact.

no PAH (Meeus et al., 2001), consistent with a flat and geometrically thin dusty disk (Malfait et al., 1998). All the previous analysis are pointing towards a disk seen nearly edge-on.

2. Observations and data reduction

51 Oph ($K = 4.3$) has been observed with AMBER, first in medium spectral resolution (MR-K, $R=1500$) with the 8m Units Telescopes (UTs) of the VLTI in September 2006, then in low resolution (LR-K, $R=35$) with the 1.8m Auxiliary Telescopes (ATs) in September 2007. The log of the observations is presented in Table 1.

Spectrally dispersed observations: The observations in medium spectral resolution have been performed in the wavelength range $[2280, 2340]\mu\text{m}$ around the CO overtone bandheads emission. On the AMBER detector are recorded both the dispersed photometry from which the spectrum of our target is derived, and the dispersed interference pattern from which the visibilities as a function of the wavelength are computed. A reference source is required to calibrate both observables (i.e. the spectrum and the visibilities).

51 Oph calibrated spectrum: In order to correct for the wavelength dependent telluric and instrumental features in the AMBER spectra, we used the observations of the calibration star HD170499. This star has a K4III spectral type and has intrinsic photospheric absorption features that need to be removed before using its observations to derive the response of the atmosphere and instrument. In particular, cool stellar photospheres show strong CO absorption longward of $2.9\mu\text{m}$ (e.g. Wallace & Hinkle (1997)). To correct for the photospheric emission we constructed a template photospheric spectrum averaging three of the best quality spectra of stars with spectral type as close as possible to our own from Wallace & Hinkle (1997): HR 1457 (K5III), HR 3275 (K4.5III), and HR 6705 (K5III). The average spectrum (normalized to the continuum) was then multiplied by the spectral slope of a K4 III star using the Pickles (1998) models available on the ISAAC web pages at ESO to obtain the template. The template spectrum was then smoothed to the AMBER spectral resolution and used to remove the photospheric signatures in the calibrator spectrum and derive the response of the system. This response was then used to correct the spectrum of

51 Oph. In Fig. 1 we show the final AMBER spectrum compared to a K band spectrum of 51 Oph obtained at the TNG telescope with the NICS NIR spectrograph (Isella, priv. comm.).

51 Oph dispersed calibrated visibilities: We computed visibilities using the standard data reduction algorithms described in Tatulli et al. (2007a), previously applying the AMDC software (Li Causi et al., 2007) to take away the spurious fringes of the detector that can bias the estimation of the visibility. A drastic fringe signal-to-noise ratio (SNR) selection using the 20% best frames was performed (for both the source and the calibrator) to insure reliable absolute calibrated visibilities (Tatulli et al., 2007a). These latter were obtained by dividing the 51 Oph raw visibilities by the reference ones, assuming a diameter of 1.28mas for the calibrator, according to the catalog of Mérand et al. (2005). Finally, we binned the spectrally dispersed visibilities in the wavelength direction in order to increase the SNR. The results are presented in Fig. 2 and the values of the visibilities in the continuum (i.e. average on the continuum spectral range) are given in Table 1.

51 Oph low resolution visibilities: LR-K data were reduced following the same procedure as the MR-K ones and then averaged spectrally to derive one single visibility of the continuum per baseline, whose values are plotted in Fig. 3 and given in Table 1 as well.

3. Modelling

Our MR-K data resolve spectrally the two CO bands (although not the rotational components within each band). For the longest baselines UT2-UT4 and UT1-UT4, the emission is spatially resolved at all wavelengths, though with rather high visibilities of 0.8. Our LR-K data are consistent with the MR-K ones, displaying high visibilities between 0.8 and 1 in the continuum at $2.2\mu\text{m}$.

To derive more information, we need to compare the observed visibilities to model predictions. We adopt simple geometrical models and describe both the continuum and bandheads emitting regions as coming from rings of constant surface brightness. At each wavelength we assume that the emission is the sum of the unresolved stellar flux F_s , of a continuum excess emission F_c and of emission in the CO bandheads F_l , with ratios that we derive from observations. In particular, the ratio $F_c/(F_s + F_c)$ is derived from the spectral energy distribution (SED) photometric data (Waters et al., 1988), fitting a Kurucz spectrum (Kurucz, 1979) for the star with $T_* = 10000\text{K}$, $R_* = 5.3R_\odot$. We find $F_c/(F_s + F_c) = 25\%$ and $F_c/(F_s + F_c) = 30\%$ at $2.2\mu\text{m}$ and $2.3\mu\text{m}$, respectively. The ratio $F_l/(F_s + F_c + F_l)$ is given by our normalized AMBER spectrum (see Fig. 1, left) in the CO bandheads and is about 18% at the peak of the 2-0 band and 19% at the peak of the 3-1 band.

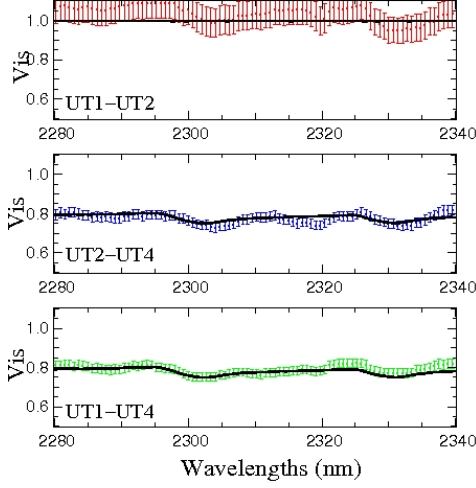
We compute two families of models, one with narrow¹ rings and one with broad rings extending from the stellar radius (in the following, uniform brightness). The parameters of the model are the inclination (i), the position angle (PA) of the system and the size of the bandheads (R_l) and continuum (R_c) emitting region, respectively. The visibility as a function of the wavelength is given by:

$$V^\lambda = \frac{F_s^\lambda + F_c^\lambda V_c^\lambda(R_c, i, PA) + F_l^\lambda V_l^\lambda(R_l, i, PA)}{F_s^\lambda + F_c^\lambda + F_l^\lambda} \quad (1)$$

¹ the width of the ring is fixed at the typical value of $\Delta R/R = 20\%$, the results being poorly dependent on its value as long as $\Delta R \ll R$.

Table 1. Log of the observations and computed absolute visibilities in the continuum.

Date	Telescopes	Baseline (m)	PA ($^{\circ}$)	Wavelength (μm)	Resolution	Calibrator	Absolute visibility
10-09-2006	U1-U2-U4	55/82/121	34/91/69	2.3	1500	HD170499	$1.0 \pm 0.1 / 0.8 \pm 0.05 / 0.8 \pm 0.03$
05-09-2007	G1-D0-H0	69/60/71	326/80/17	2.2	35	HD163955	$0.8 \pm 0.1 / 0.85 \pm 0.1 / 1.0 \pm 0.1$
05-09-2007	G1-D0-H0	65/46/70	345/89/24	2.2	35	HD163955	$1.0 \pm 0.15 / 1.0 \pm 0.1 / 0.87 \pm 0.1$
06-09-2007	G1-D0-H0	64/31/67	0/98/27	2.2	35	HD172051	$0.85 \pm 0.12 / 0.95 \pm 0.1 / 0.95 \pm 0.1$

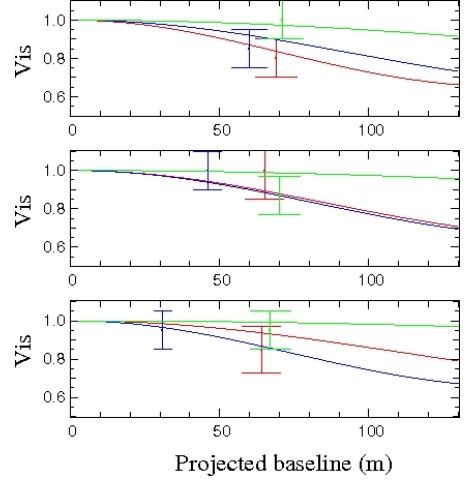
**Fig. 2.** MR-K calibrated visibilities as a function of the wavelengths for the three baselines and overplotted best model (black thick line), for the ring case.**Table 2.** Best-fit model parameters.

Model	χ^2_{min}	i ($^{\circ}$)	PA ($^{\circ}$)	R_c (AU)	R_l (AU)
Uniform Brightness	0.8	85^{+5}_{-15}	129^{+10}_{-9}	$0.43^{+0.10}_{-0.15}$	$0.36^{+0.06}_{-0.07}$
Narrow Ring	0.8	82^{+8}_{-15}	126^{+15}_{-5}	$0.24^{+0.06}_{-0.03}$	$0.15^{+0.07}_{-0.04}$

where V_c^{λ} is the visibility of the region emitting the continuum and V_l^{λ} that of the region emitting the bandheads.

Fitting together the continuum and bandheads models, we have performed a least-square minimization test on a large grid of parameters varying both radii from 0 to 3AU, the inclination from 0 to 90 $^{\circ}$ and the position angle from 0 to 180 $^{\circ}$. The χ^2 function presents a clear and unambiguous minimum, for two reasons: (i) the high value of the visibilities imposing that we are in the first lobe of the visibility function, hence that the emission regions are rather compact and, (ii) the broad range of baseline orientations which put strong constraints on the inclination and the position angle of the system. The parameters of the best-fit model are summarized in Table 2, and the result of the fit is shown in Fig. 2 and 3, for the narrow ring model case.

We note that both the bandheads and continuum components are unresolved for the smallest UT baseline shown in the top panel of Fig. 2. This suggests that the small variations of the visibility detected in the CO bandheads are probably remaining biases of the data reduction, given the low SNR of the interferograms. However, considering the error bars of the measurements, this (possible) bias has only a very marginal influence on the sizes we derive and does not impact on their interpretation.

**Fig. 3.** LR-K calibrated visibilities as a function of the projected baselines, for the three observations, and overplotted best model (lines). In each panel, colors red, blue, and green correspond to baselines G1-D0, D0-H0, and G1-D0 respectively.

4. Discussion

4.1. Sizes of emitting regions vs. modelling

The uniform brightness and the narrow ring are the two extreme cases of a unique model of uniform distribution in which the width of the emitting region is varying. We emphasize that this geometrical modelling defines the metric that allows us to unequivocally link the measured visibilities to the spatial brightness distribution of these regions, through the Zernicke-Van Cittert theorem (Goodman, 1985). It does not introduce assumptions regarding the mechanisms at the origin of these emissions. We present in Table 2 the results for the two scenarios. All the intermediate models would also work, with intermediate values for the sizes. Note that the uniform brightness returns the largest size because emission is added at small spatial scales down to the stellar radius. The uniform brightness has no proper physical meaning since neither the dust nor the CO gas can survive so close to the star. However, it represents the *characteristic size* of the emission region. As this quantity is commonly used in infrared interferometry, it is given here for this purpose. Conversely the narrow ring model is sensitive to the location where most of the emission is arising from, usually the *inner rim* of this emission. In the following, we will analyze our results in the light of the narrow ring only. We emphasize that the size of the CO emitting region is *smaller than the one of the continuum*, independently of the choice of our model.

4.2. Inclination and position angle of the system

We find a position angle of 126^{+15}_{-5} degrees and an inclination of $i = 82^{+8}_{-15}$ degrees. This inclination is in agreement with most of the previous studies. Berthoud et al. (2007) have, however,

proposed an alternative scenario in which the object would have an inclination lower than 36° . Our measurements are positively ruling out this latter option.

4.3. Locating the CO bandheads emission region

For the first time, we are spatially resolving the CO bandheads emission region in 51 Oph. We find that most of the CO bandheads are emitted at a radius of $R_l = 0.15^{+0.07}_{-0.04}$ AU from the central star. This is fully supporting the scenario in which the CO bandheads emission is arising from the inner region of a hot gaseous disk in Keplerian rotation, between 0.15 AU and 0.35 – 0.53 AU, as derived from spectroscopic modelling of the CO bandheads (Thi et al., 2005; Berthoud et al., 2007), and where the temperature is hot enough (≥ 2000 K) to excite the first overtone bands at $2.3 \mu\text{m}$. More precisely, these authors, though they are fitting the CO bandheads with a broad ring, are pointing out that most of the emission comes from a region close to the inner radius of their gaseous disk model at ~ 0.15 AU. This is in excellent agreement with the value we derive in the present analysis. We note that one single ring enables us to reproduce the visibility in the two bandheads, indicating that both the 2-0 and 3-1 bands come from the same physical region. We also note that the CO emission region is inside the near infrared continuum one, the latter being located at a radius of $R_c = 0.24^{+0.06}_{-0.03}$ AU. This result corroborates that the CO is emitted from a dust free region, regardless of the true origin of the continuum (see Sect. 4.4). At such a distance from the star, the survival of the CO gas from photo-dissociation must however be considered. Thi et al. (2005) suggested that two mechanisms can circumvent the photo-dissociation process: the self-shielding of the CO molecules that occurs if the column density is high enough ($N(\text{CO}) > 10^{15} \text{ cm}^{-2}$, van Dishoeck & Black (1988)), as well as the $\text{C} + \text{OH} \rightarrow \text{CO} + \text{H}$ chemical reaction, which insures a continuous replenishment of this molecule.

4.4. The origin of the continuum near-infrared excess

The continuum excess of 51 Oph is weak and, according to the shape of its SED (Waters et al., 1988), appears to come from a small and tenuous disk of dust which is optically thin at most wavelengths, as already inferred by Malfait et al. (1998). We performed SED fitting with the MCFOST dusty disk code of Pinte et al. (2006), and found the same results with a low amount of dust present in the disk ($M_{\text{dust}} \sim 10^{-8} M_\odot$). The result of our modelling is shown in Fig. 4. This model however requires a dust inner edge located at the dust sublimation radius, which in the case of 51 Oph would be at $R_{\text{dust}} \sim 1.2$ AU for a typical grain size distribution of spherical particles² and a dust sublimation temperature of $T_{\text{dust}} \sim 1500$ K. Obviously this model, with such a large inner rim, is not compatible with our measured visibilities as shown by Fig. 5, and for which we calculate a χ^2 of ~ 10 . Studying the extreme case where only big grains are present would shrink the dust sublimation radius down to $R_{\text{dust}} \sim 0.56$ AU, still at least two times further out than the distance suggested by our data. Interestingly, a similar problem was evidenced by Leinert et al. (2004) on the same star, the 0.5 AU mid-infrared size of 51 Oph derived from their MIDI measurements being too small to be compatible with the shape of the SED.

Several scenarios may however circumvent this apparent dis-

² $dn(a) \propto a^{-3.7} da$, ranging from $a_{\text{min}} = 0.03 \mu\text{m}$ to $a_{\text{max}} = 1 \text{ mm}$, with optical constants from Mathis & Whiffen (1989)

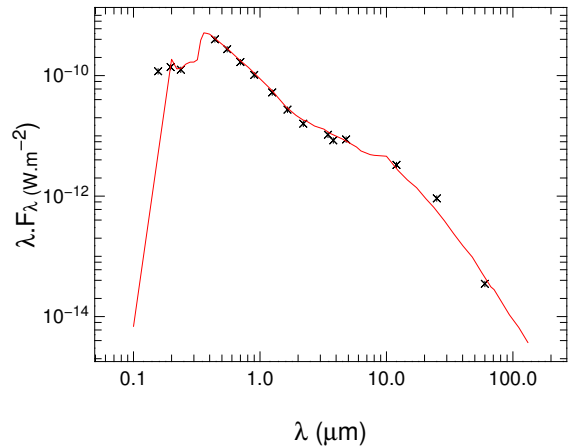


Fig. 4. Spectral energy distribution of 51 Oph taken from literature (Waters et al., 1988) (crosses) and superimposed best fit model (solid line) using MCFOST dusty disk model. The main parameters that are fitted are the inner radius $R_{\text{dust}} = 1.2$ AU, the outer radius $R_{\text{out}} = 400$ AU scale height at 1 AU $H_0 = 0.04$, the flaring exponent $\beta = 1.1$, the grain size distribution (see text), the surface density exponent $p = -1.25$ and the total mass of dust $M_{\text{dust}} = 10^{-8} M_\odot$. We refer to Pinte et al. (2006) for a thorough description of the modelling.

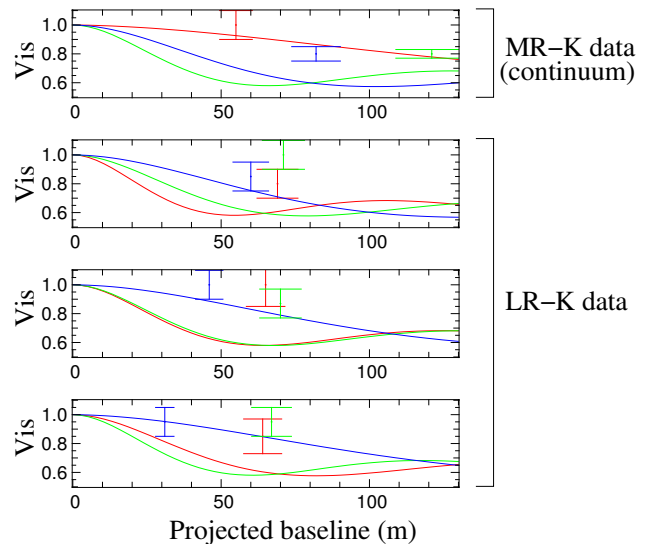


Fig. 5. MR-K continuum visibilities (top panel) and LR-K visibilities as a function of the baseline and overplotted MCFOST model arising from SED fitting (lines). The color code is the same than in fig. 2 and 3. We can see that this model, with inner radius equal to the dust sublimation radius, is incompatible with the interferometric data, with a resulting χ^2 of ~ 10 .

agreement of the location of the dust evaporation radius with respect to our derived inner edge position. First, the gas inside the dust sublimation may help the dust to survive closer in by absorbing a fraction of the stellar radiation available to heat the dust. According to Muzerolle et al. (2004), the gas accreting onto the star becomes optically thick to stellar radiation for accretion rates higher than $\dot{M} \sim 10^{-7} M_\odot/\text{yr}$. The accretion rate of $1 - 2 \cdot 10^{-7} M_\odot/\text{yr}$ derived from Bry luminosity would actually place the gas in 51 Oph at the frontier between the optically thin and optically thick regimes.

Another possibility comes from the rapidly rotating nature of 51

Oph. Given its measured rotational velocity $v \sin i = 270 \text{ km/s}$ (Dunkin et al., 1997), and knowing that this star is seen almost edge-on, 51 Oph would rotate at 90% of its critical velocity given by $v_{crit} = \sqrt{2GM_*/(3R_*)} \approx 300 \text{ km/s}$. Therefore, 51 Oph is likely elongated with a drop of its gravity (g_{eff}) from pole to equator, and subsequently of its effective temperature (von Zeipel, 1924). The star being cooler at the equator than at the poles, the dust distributed in the equatorial plane will be heated less efficiently and the evaporation radius moved closer to the star. From the gravity darkening law $T_{eff}^4 \propto g_{eff}$ (solid body approximation), the effective temperature of 51 Oph at the equator can be estimated to be of the order of 75% of that of the pole, hence lowering the sublimation radius by a factor of 2.

Finally, one last explanation would be that the infrared excess is not entirely originating from dust thermal emission. The gas inside the dust sublimation radius could substantially contribute to the near infrared energy balance. Muzerolle et al. (2004) have shown that inner optically thick gaseous zones are indeed expected to emit a large continuum excess in the near infrared through free-free emission. Interestingly, this effect has been recently shown to take place in Herbig Ae/Be stars (Eisner et al., 2007; Isella et al., 2008; Tannirkulam et al., 2008).

4.5. 51 Oph: a classical Be star?

51 Oph appears to be a peculiar source in an unusual transitional state. In the frame of Herbig Ae/Be stars, its SED presents a near infrared excess which is too small to account for a classical puffed-up inner rim. In the frame of β -Pic like stars, 51 Oph is also lacking the far infrared-excess bump associated with the presence of an outer dusty disk, the inner disk being emptied by a potential forming planet (Malfait et al., 1998). Instead these authors suggest that 51 Oph is undergoing an alternative evolution scheme, without forming planets. Furthermore, the presence of strong CO overtone emission bandheads also makes 51 Oph quite a puzzling case. Such emission requires large column densities of warm gas in order to produce detectable emission. Such large column densities are rare except in sources with the largest accretion rates (Najita et al., 2007). Interestingly, the CO overtone has also been detected in the B9 star HD58647 (Berthoud, 2008), for which the SED profile is similar to that of 51 Oph (Malfait et al., 1998). In HD58647 however, there is less CO emission but its infrared excess is stronger. Berthoud (2008) thus concluded that both stars are most likely classical Be stars surrounded by massive gaseous disk, though seen at different evolutionary stages. This scenario is in agreement with their high rotational velocities ($v \sin i = 270 \text{ km/s}$ and 118 km/s for 51 Oph and HD58647 respectively) and gives credit to the hypothesis that most of the near infrared continuum emission – if not all – is arising from the circumstellar gas. HD58647 has been observed with the Keck interferometer (Monnier et al., 2005) and these authors have derived a rather compact size of 0.4 AU for its near infrared continuum emission, slightly larger as that of 51 Oph for an equivalent luminosity ($L = 260 L_\odot$ for 51 Oph vs. $L = 250 L_\odot$ for HD58647). This is again below – or at the very lower limit of – the dust sublimation radius, pointing towards the same gaseous origin for the continuum than that of 51 Oph. Hence, the very inner environment of this type of stars seems to follow an intriguing evolution scheme where the dust progressively dissipates leaving behind a massive gas-rich, strongly accreting disk. As the hot dust is vanishing, the relative contribution of the gas to the continuum infrared excess increases, its region of emission moving closer to the star. How the circum-

stellar dust disappears remains rather unclear. Repeated studies combining spectroscopic detection of emission bandheads (CO, hydrogen) and interferometric measurements in a large sample of stars would certainly help improve our understanding on how these disks are evolving and dissipating.

5. Summary

The principal results are summarized here:

- using the AMBER/VLTI interferometer, we have spatially and spectrally resolved the CO bandheads emission at $2.3 \mu\text{m}$
- the inclination of the system is constrained by our observations, and we confirm that the object is seen nearly edge-on.
- assuming simple ring models for the distribution of both the near infrared continuum and CO emissions, we locate the bandheads emission region at a distance of $0.15_{-0.04}^{+0.07} \text{ AU}$ from the star, inside the continuum emission region, reinforcing the scenario in which the CO bandheads originate from the inner part of a dust free gaseous disk.
- the continuum emission is located at a distance of $0.24_{-0.03}^{+0.06} \text{ AU}$, at least two times closer to the star than the dust sublimation radius. This suggests that the inner disk of gas is playing an important role, whether by shielding the star light and thus allowing the dust to survive closer to the star, and/or by contributing to a non negligible part of the near infrared continuum emission.

Acknowledgements. Authors would like to thank C. Pinte and G. Duchêne for fruitful discussions concerning the disk modelling using the MCFOST software. This project was partially supported by the PRIN INAF 2006 grant "From Disks to Planetary Systems". At LAOG E.T. is supported by a postdoc grant from CNRS/INSU, France. This research is supported by *Agence Nationale de la Recherche* (ANR) of France through contract ANR-07-BLAN-0221 and by *Programme National de Physique Stellaire* (PNPS) of CNRS/INSU, France. A.N. and L.T. were partially supported by the INAF 2005 grant "Interferometria infrarossa: ottimizzazione di osservazioni astrofisiche" and by the INAF 2006 grant "From Disks to Planetary Systems".

References

- Berthoud, M. G., Keller, L. D., Herter, T. L., Richter, M. J., & Whelan, D. G. 2007, *ApJ*, 660, 461
- Berthoud, M. G. 2008, Ph.D. Thesis
- Bouwman, J., Meeus, G., de Koter, A., Hony, S., Dominik, C., & Waters, L. B. F. M. 2001, *A&A*, 375, 950
- Brittain, S. D., Simon, T., Najita, J. R., & Rettig, T. W. 2007, *ApJ*, 659, 685
- Dunkin, S. K., Barlow, M. J., & Ryan, S. G. 1997, *MNRAS*, 290, 165
- Eisner, J. A. 2007, *Nature*, 447, 562
- Eisner, J. A., Chiang, E. I., Lane, B. F., & Akeson, R. L. 2007, *ApJ*, 657, 347
- Garcia Lopez, R., Natta, A., Testi, L., & Habart, E. 2006, *A&A*, 459, 837
- Goodman, J. W. 1985, New York: Wiley, 1985.
- Isella, A., Tatulli, E., Natta, A., & Testi, L. 2008, *A&A*, 483, L13
- Kraus, S., et al. 2008, accepted
- Kurucz, R. L. 1979, *ApJS*, 40, 1
- Lagage, P. O., & Pantin, E. 1994, *Experimental Astronomy*, 3, 57
- Leinert, C., et al. 2004, *A&A*, 423, 537
- Li Causi, G., Antonucci, S., & Tatulli, E. 2008, *A&A*, 479, 589
- Liu, W. M., Hinz, P. M., Meyer, M. R., Mamajek, E. E., Hoffmann, W. F., Brusa, G., Miller, D., & Kenworthy, M. A. 2007, *ApJ*, 658, 1164
- Malbet, F., et al. 2007, *A&A*, 464, 43
- Malfait, K., Bogaert, E., & Waelkens, C. 1998, *A&A*, 331, 211
- Mathis, J. S., & Whiffen, G. 1989, *ApJ*, 341, 808
- Meeus, G., Waters, L. B. F. M., Bouwman, J., van den Ancker, M. E., Waelkens, C., & Malfait, K. 2001, *A&A*, 365, 476
- Mérand, A., Bordé, P., & Coudé Du Foresto, V. 2005, *A&A*, 433, 1155
- Monnier, J. D., et al. 2005, *ApJ*, 624, 832
- Muzerolle, J., D'Alessio, P., Calvet, N., & Hartmann, L. 2004, *ApJ*, 617, 406
- Najita, J. R., Carr, J. S., Glassgold, A. E., & Valenti, J. A. 2007, *Protostars and Planets V*, 507
- Pickles, A. J. 1998, *PASP*, 110, 863

- Pinte, C., Ménard, F., Duchêne, G., & Bastien, P. 2006, *A&A*, 459, 797
Tatulli, E., et al. 2007, *A&A*, 464, 29
Tatulli, E., et al. 2007, *A&A*, 464, 55
Tannirkulam, A., et al. 2008, *ApJ*, 677, L51
Thi, W.-F., van Dalen, B., Bik, A., & Waters, L. B. F. M. 2005, *A&A*, 430, L61
van Dishoeck, E. F., & Black, J. H. 1988, *ApJ*, 334, 771
von Zeipel, H. 1924, *MNRAS*, 84, 684
Wallace, L., & Hinkle, K. 1997, *ApJS*, 111, 445
Waters, L. B. F. M., Cote, J., & Geballe, T. R. 1988, *A&A*, 203, 348